Electronic Supplementary Information for

Repurposing e-waste cathodes as catalysts for CO_2 reduction *via* the reverse water-gas shift reaction

*Zhihao Zhou, Siyuan Duan, Guangze Nie, Zhenkun Sun *, Lunbo Duan **

Key Laboratory of Energy Thermal Conversion and Control of Ministry of Education, School of Energy and Environment, Southeast University, Nanjing, 211189, China

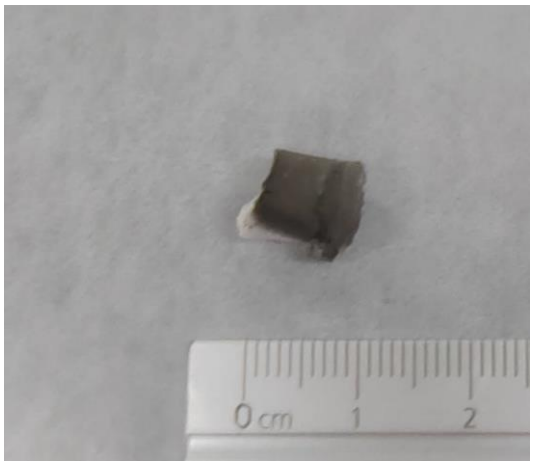

Fig. S1 Optical photo of NCM sample after reduction under 4 *vol*% H_2/N_2 at 600 °C for 30 min

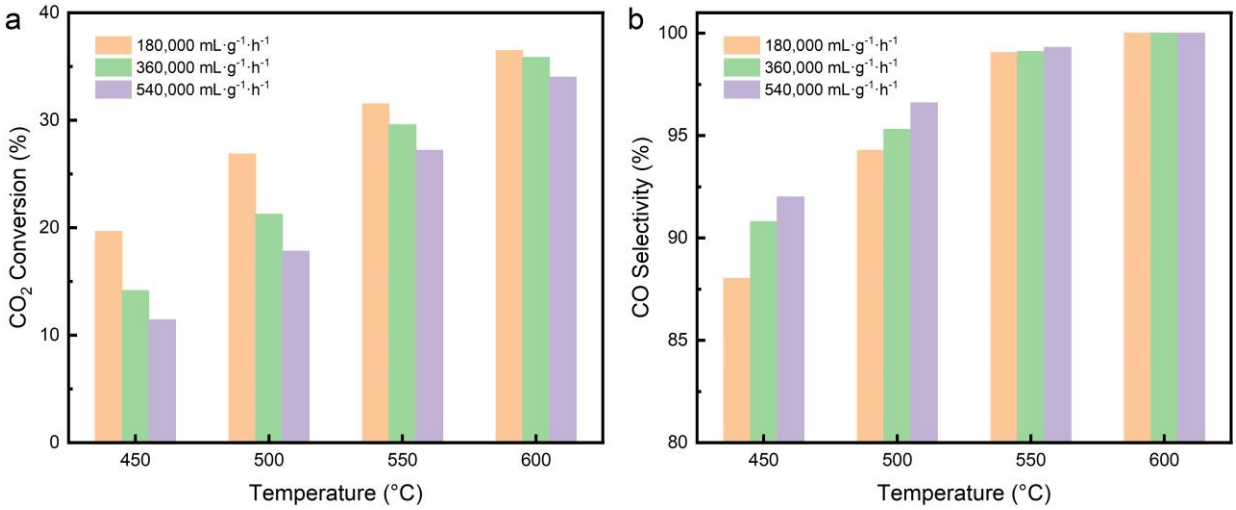

Fig. S2 (a) CO_2 conversion and (b) CO selectivity of the RWGS reaction over the 10NCM/Al_2O_3 catalyst at 450–600 °C under GHSV withing 180,000–540,000 mL·g^{-1}·h^{-1}.

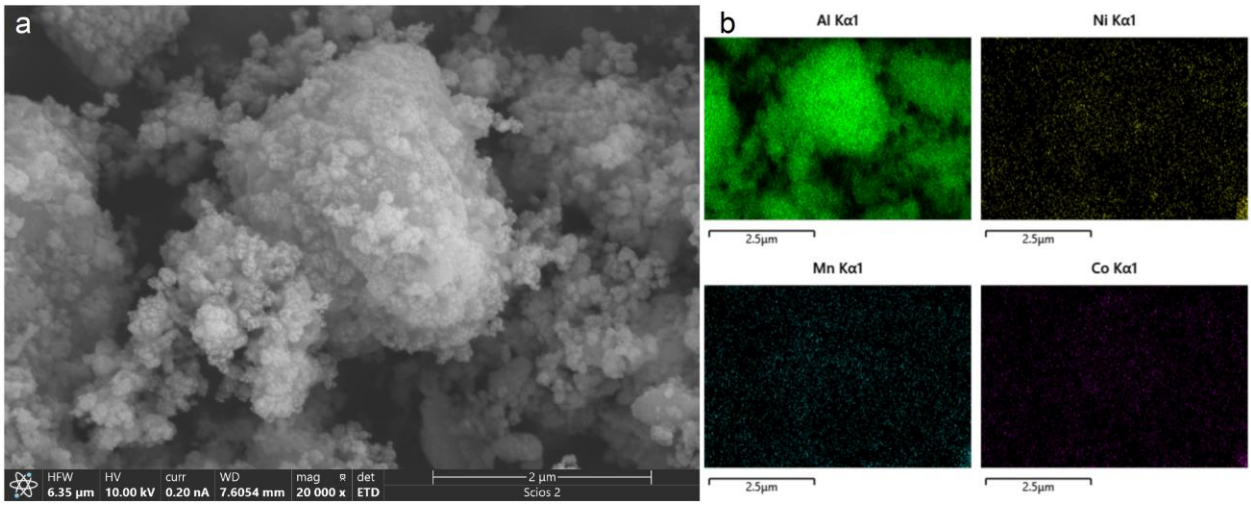

Fig. S3 (a) SEM image and (b) EDS element mappings of the freshly prepared 10NCM/Al_2O_3 catalyst.

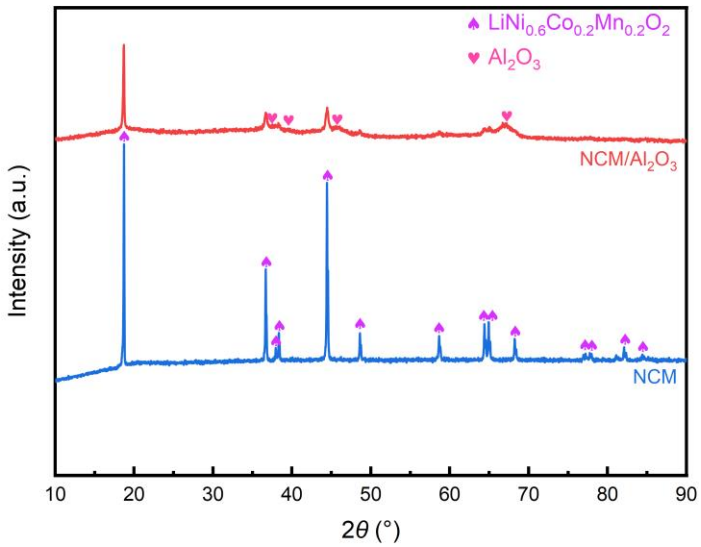

Fig. S4 XRD patterns for the freshly prepared 10NCM/Al_2O_3 catalyst, and NCM sample.

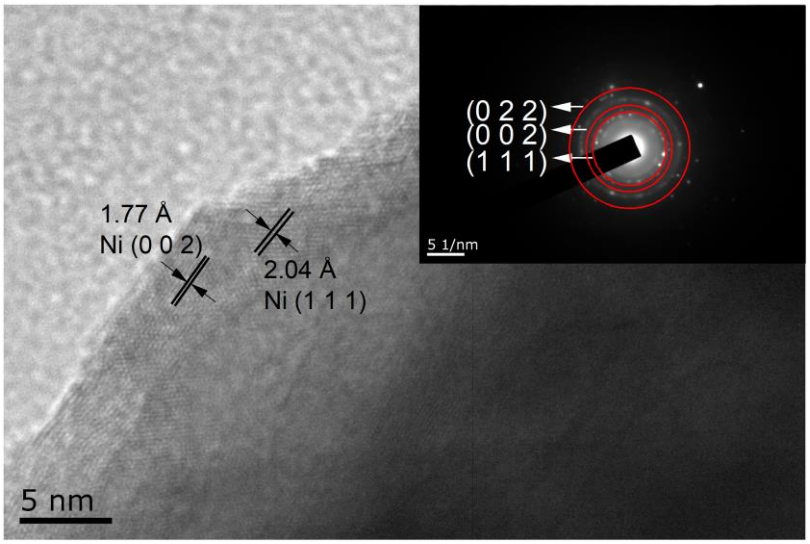

Fig. S5 HR-TEM image of the reduced 10NCM/Al_2O_3 catalysts (inset: selected area electron diffraction image).

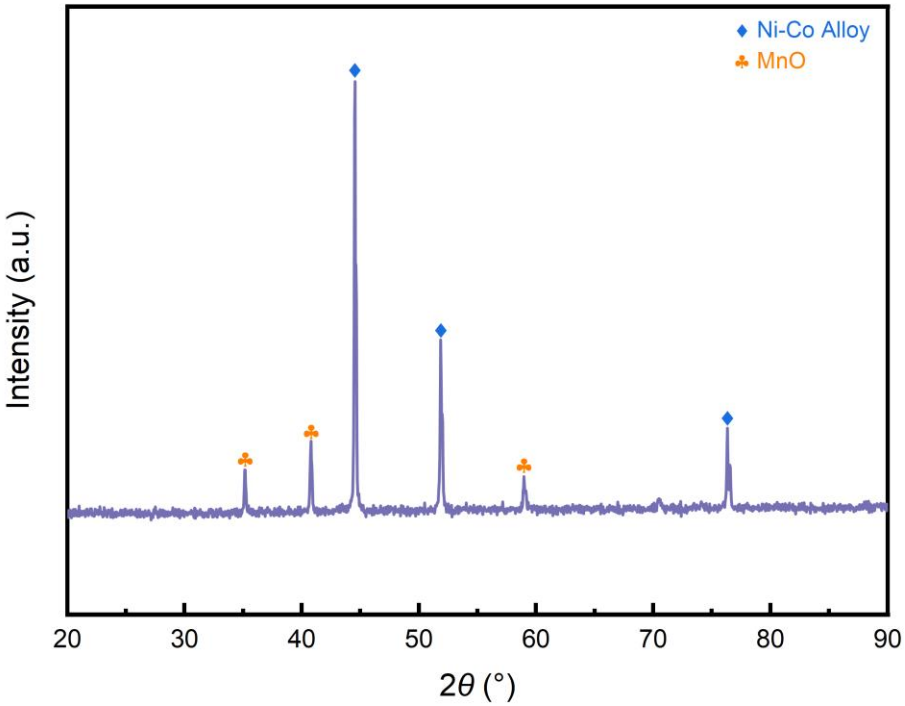

Fig. S6 XRD pattern for the fully reduced NCM sample.

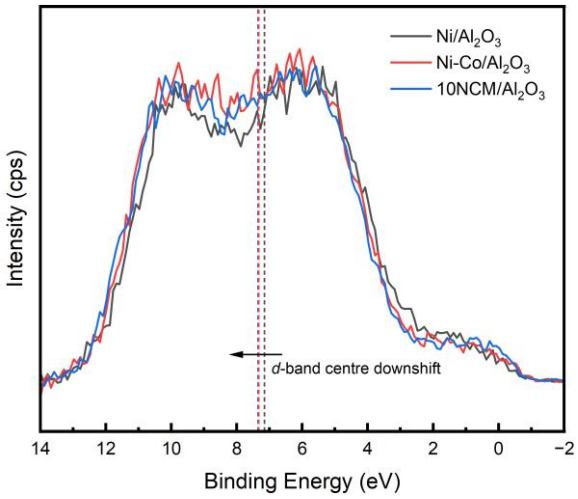

Fig. S7 Valence band spectra of the reduced Ni/Al_2O_3, $Ni\text{-}Co/Al_2O_3$ and $10NCM/Al_2O_3$ catalysts.

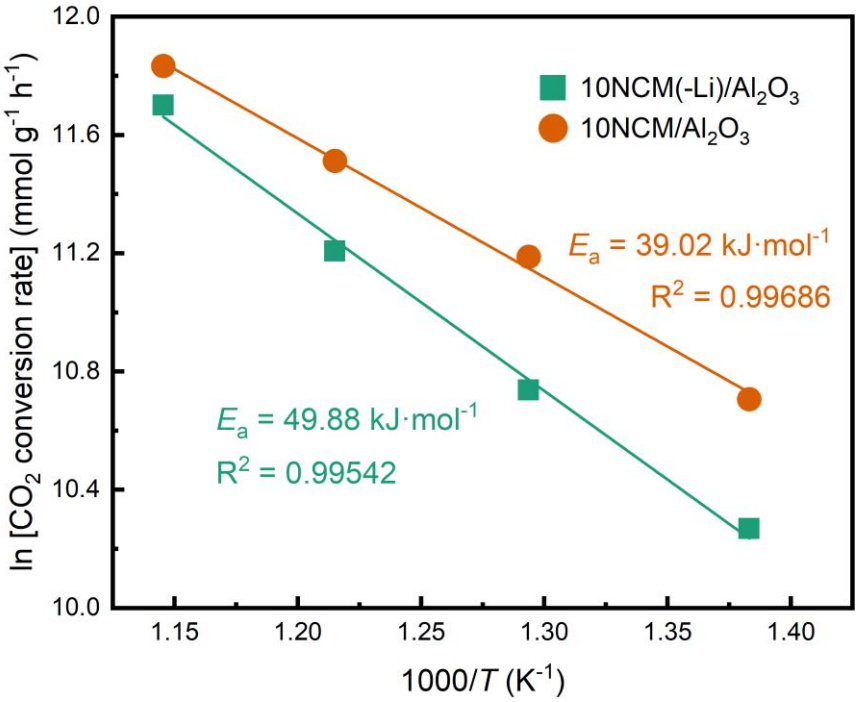

Fig. S8 Arrhenius plots of the CO_2 conversion rate during the RWGS reaction over the 10NCM/Al_2O_3 and 10NCM(-Li)/Al_2O_3 catalysts at 450-600 °C.

Table S1 Elemental compositions of the NCM and NCM(-Li) samples (*wt*.%).

Sample	Li	Ni	Co	Mn
NCM	9.2	41.7	14.0	12.8
NCM(-Li)	0.6	46.3	13.7	13.1

Table S2 Elemental compositions of the oxidised M/Al_2O_3 catalysts (*wt*%).

Catalyst	Al	Ni	Co	Mn
Ni/Al_2O_3	58.3	9.4	-	-
Co/Al_2O_3	59.5	-	6.7	-
$Ni\text{-}Co/Al_2O_3$	60.1	6.6	2.4	-
$Ni\text{-}Co\text{-}Mn/Al_2O_3$	60.5	6.0	2.1	2.0

Table S3 Summary of the optimal results of present work and relevant recent reports.

Catalyst	GHSV ($mL \cdot g^{-1} \cdot h^{-1}$)	Temperature (°C)	CO_2 conversion (%)	R value *	CO selectivity (%)	Reference
$H_2/CO_2 = 1$						
NCM/Al_2O_3	180 000	450	20	0.833	88	This work
		500	27	0.931	95	
		550	32	0.941	99	
		600	36	0.960	100	
Fe_3O_4	10 667	450	14	0.583	98	1
		500	17	0.586	97	
		550	22	0.647	97	
CuFe/Al_2O_3	200 000	450	8	0.333	99	2
		500	11	0.379	99	
		550	14	0.412	99	
		600	18	0.474	99	
Ni/SBA-16	36 000	500	21	0.724	91	3
MoO_3/FAU	7 500	500	14	0.483	99	4
CuO/FAU	7 500	500	7	0.241	98	
Fe_3O_4/FAU	7 500	500	6	0.207	98	
NiO/FAU	7 500	500	17	0.586	45	
Cu-MoO_3/FAU	7 500	450	15	0.625	99	
		500	19	0.655	99	
		550	23	0.676	99	
Pd-In/SiO_2	60 000	450	0.2	0.008	100	5
		500	0.6	0.021	100	
		550	3	0.088	100	
		600	9	0.237	100	
Pd/SiO_2	60 000	450	8	0.333	46	
		500	16	0.552	39	
		550	23	0.676	55	
		600	29	0.806	82	
$La_{0.75}Sr_{0.25}FeO_3$	37 500	550	16	0.471	95	6
Pt/ZSM-5	30 000	450	0.8	0.033	96	7
		500	2	0.069	95	
Pt/KLTL	30 000	450	7	0.292	99	
		500	13	0.448	97	
K-Pt/KLTL	30 000	450	21	0.875	100	
		500	27	0.931	100	
Pt/mullite	30 000	450	10	0.417	92	8
		500	16	0.551	88	

		550	23	0.676	84	
K-Pt/mullite	30 000	450	21	0.875	100	
		500	26	0.897	99	
		550	31	0.912	98	
Pt-K/mullite	30 000	450	22	0.917	100	
		500	27	0.931	99	
		550	31	0.912	98	
$H_2/CO_2 = 3$						
$CuAl_2O_4$	9 960	450	28	0.560	99	9
		500	33	0.647	99	
Pt/Fe_3O_4	432 000	500	35	0.680	99	10
$H_2/CO_2 = 4$						
Mo-P-SiO_2	12 000	450	5.8	0.092	100	11
		500	13	0.224	97	
		550	21	0.350	100	
		600	34	0.523	92	
Mo-P-Al_2O_3	12 000	450	8.4	0.133	77	
		500	16	0.276	86	
		550	26	0.433	83	
		600	39	0.600	83	
Mo-P-CeAl	12 000	450	6.8	0.108	100	
		500	14	0.241	89	
		550	25	0.417	88	
		600	35	0.538	86	
Fe-Cu/CeO_2-Al_2O_3	60 000	450	51	0.810	100	12
		500	56	0.966	100	
Co@SiO_2	15 000	450	48	0.762	19	13
		500	51	0.879	27	
		550	53	0.883	43	
		600	57	0.877	61	
NiCo@SiO_2	15 000	450	46	0.730	49	
		500	50	0.862	50	
		550	54	0.900	55	
		600	60	0.923	70	

* R value is defined as the ratio of experimental CO_2 conversion to equilibrium CO_2 conversion.[1]

Table S4 CO_2 conversion and CO selectivity of RWGS reaction over 10NCM523/Al_2O_3 and 10NCM811/Al_2O_3 catalysts at 450–600 °C.

Catalyst	Temperature (°C)	CO_2 conversion (%)	CO selectivity (%)
10NCM523/Al_2O_3	450	18	89
	500	25	95
	550	31	100
	600	35	100
10NCM811/Al_2O_3	450	20	88
	500	28	94
	550	32	99
	600	37	100

References

(1) Kumar, V.; Lamba, N. K.; Baig, A.; Kaushik, J.; Jha, T.; Sonal; Sonkar, S. K. Utilization of steel industry waste derived magnetic iron-oxide nanoparticles for reverse water gas shift reaction. *Chem. Eng. J.* **2023**, *477*, 147027. DOI: 10.1016/j.cej.2023.147027.

(2) Pahija, E.; Panaritis, C.; Rutherford, B.; Couillard, M.; Patarachao, B.; Shadbahr, J.; Bensebaa, F.; Patience, G. S.; Boffito, D. C. FeO_x nanoparticle doping on Cu/Al_2O_3 catalysts for the reverse water gas shift. *J. CO2 Util.* **2022**, *64*, 102155. DOI: 10.1016/j.jcou.2022.102155.

(3) Chen, C.-S.; Budi, C. S.; Wu, H.-C.; Saikia, D.; Kao, H.-M. Size-Tunable Ni Nanoparticles Supported on Surface-Modified, Cage-Type Mesoporous Silica as Highly Active Catalysts for CO_2 Hydrogenation. *ACS Catal.* **2017**, *7* (12), 8367-8381. DOI: 10.1021/acscatal.7b02310.

(4) Okemoto, A.; Harada, M. R.; Ishizaka, T.; Hiyoshi, N.; Sato, K. Catalytic performance of MoO_3/FAU zeolite catalysts modified by Cu for reverse water gas shift reaction. *Appl. Catal. A: Gen.* **2020**, *592*, 117415. DOI: 10.1016/j.apcata.2020.117415.

(5) Ye, J.; Ge, Q.; Liu, C. Effect of PdIn bimetallic particle formation on CO_2 reduction over the Pd–In/SiO_2 catalyst. *Chem. Eng. Sci.* **2015**, *135*, 193-201. DOI: 10.1016/j.ces.2015.04.034.

(6) Daza, Y. A.; Kuhn, J. N. CO_2 conversion by reverse water gas shift catalysis: comparison of catalysts, mechanisms and their consequences for CO_2 conversion to liquid fuels. *RSC Adv.* **2016**, *6* (55), 49675-49691, 10.1039/C6RA05414E. DOI: 10.1039/C6RA05414E.

(7) Yang, X.; Su, X.; Chen, X.; Duan, H.; Liang, B.; Liu, Q.; Liu, X.; Ren, Y.; Huang, Y.; Zhang, T. Promotion effects of potassium on the activity and selectivity of Pt/zeolite catalysts for reverse water gas shift reaction. *Appl. Catal. B: Environ.* **2017**, *216*, 95-105. DOI:

10.1016/j.apcatb.2017.05.067.

(8) Liang, B.; Duan, H.; Su, X.; Chen, X.; Huang, Y.; Chen, X.; Delgado, J. J.; Zhang, T. Promoting role of potassium in the reverse water gas shift reaction on Pt/mullite catalyst. *Catal. Today* **2017**, *281*, 319-326. DOI: 10.1016/j.cattod.2016.02.051.

(9) Kang, H.-F.; Liu, Y.-J.; Lu, Y.; Zhang, P.; Tang, M.-X.; Gao, Z.-X.; Ge, H.; Fan, W.-B. Exploring the sustained release catalysis of $CuAl_2O_4$ spinel for highly effective CO_2 conversion to CO. *J. Catal.* **2024**, *432*, 115427. DOI: 10.1016/j.jcat.2024.115427.

(10) Chen, H.; Zhao, Z.; Wang, G.; Zheng, Z.; Chen, J.; Kuang, Q.; Xie, Z. Dynamic Phase Transition of Iron Oxycarbide Facilitated by Pt Nanoparticles for Promoting the Reverse Water Gas Shift Reaction. *ACS Catal.* **2021**, *11* (23), 14586-14595. DOI: 10.1021/acscatal.1c03772.

(11) Zhang, Q.; Bown, M.; Pastor-Pérez, L.; Duyar, M. S.; Reina, T. R. CO_2 Conversion via Reverse Water Gas Shift Reaction Using Fully Selective Mo–P Multicomponent Catalysts. *Ind. Eng. Chem. Res.* **2022**, *61* (34), 12857-12865. DOI: 10.1021/acs.iecr.2c00305.

(12) Yang, L.; Pastor-Pérez, L.; Villora-Pico, J. J.; Sepúlveda-Escribano, A.; Tian, F.; Zhu, M.; Han, Y.-F.; Ramirez Reina, T. Highly Active and Selective Multicomponent Fe–Cu/CeO_2–Al_2O_3 Catalysts for CO_2 Upgrading via RWGS: Impact of Fe/Cu Ratio. *ACS Sustain. Chem. Eng.* **2021**, *9* (36), 12155-12166. DOI: 10.1021/acssuschemeng.1c03551.

(13) Price, C. A. H.; Pastor-Perez, L.; Reina, T. R.; Liu, J. Yolk-Shell structured NiCo@SiO_2 nanoreactor for CO_2 upgrading via reverse water-gas shift reaction. *Catal. Today* **2022**, *383*, 358-367. DOI: 10.1016/j.cattod.2020.09.018.